NANO LETTERS

Letter

pubs.acs.org/NanoLett

Local Mapping of Generation and Recombination Lifetime in $BiFeO_3$ Single Crystals by Scanning Probe Photoinduced Transient Spectroscopy

Marin Alexe*

Max Planck Institute of Microstructure Physics, Weinberg 2, 06120 Halle, Germany

Supporting Information

ABSTRACT: Carrier lifetime in photoelectric processes is the average time an excited carrier is free before recombining or trapping. Lifetime is directly related to defects and it is a key parameter in analyzing photovoltaic effects in semiconductors. We show here a scanning probe method combined with photoinduced current spectroscopy that allows mapping with nanoscale resolution of the generation and recombination lifetimes. Using this method we have analyzed the mechanism of the abnormal photovoltaic effect in multiferroic bismuth ferrite, $BiFeO_3$. We found that generation and recombination lifetimes in $BiFeO_3$ are large due to complex generation and recombination processes that involve shallow energy levels in the band gap. The domain walls do not play a major role in the photovoltaic mechanism.

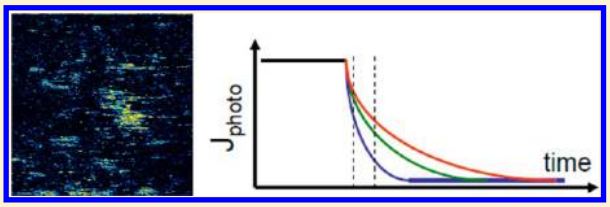

KEYWORDS: *Photovoltaic, multiferroic, BiFeO3, scanning probe, photoinduced transient spectroscopy, lifetime*

Bismuth ferrite is known as one of the few perovskite oxides showing multiferroic properties at room temperature.[1] Recently this intricate material has shown another interesting face namely the semiconductor properties. Its band gap of only 2.7 eV, lying in the blue region of the visible spectrum, is noticeably lower than that of the other well-known ferroelectrics such as $LiNbO_3$, $BaTiO_3$, $Pb(Zr,Ti)O_3$, and so forth making $BiFeO_3$ (BFO) attractive for studies of photoelectric effects. Photoinduced effects in BFO single crystals such as photoinduced expansion[2] and switchable diode[3,4] have been already demonstrated. But, perhaps the most interesting and one with high application potential is the abnormal photovoltaic effect exhibited by epitaxial thin BFO films with ordered domain patterns.[5] Open circuit photovoltages (OCV) as large as 15 V have been measured on these high quality films by illumination with light having the photon energy above the band gap, whereas single domain films or metal−BFO−metal structures show OCV lower than the bandgap.[6] The origin of the abnormal photovoltaic effect was supposed to be the ferroelectric domain walls. It was assumed and later on theoretically analyzed[7] that the strong local electrical field existing at the domain walls will separate the electron−hole pairs (ehp) photogenerated within the domain wall whereas the carriers will strongly recombine within the bulk of the domains. The separated electrons and holes will accumulate only at the domain walls, building in such way a small voltage across each domain wall. At the macroscopic level, the voltages will sum up and generate the large open circuit voltage. This mechanism based entirely on the domain walls is different from the bulk photovoltaic effect, known to exist in materials lacking inversion symmetry.[8] If the photovoltaic mechanism based on domain walls, which represent only few percent of the whole volume of the system, would be proven to be valid, it will open the possibility to engineer a totally new class of devices in which a tiny volume of a material can generate giant photoelectric currents and voltages. In order to gain insight into this mechanism, one has to develop measurement methods that will allow local mapping of essential photoelectronic quantities, such as the effective carrier lifetime, with a spatial resolution of the same order of magnitude as the domain walls, that is, 3−5 nm. Recently, noncontact scanning probe microscopy (SPM) methods, that is, electrostatic force and Kelvin probe microscopy, have been employed to study photogenerated charge carriers in organic polymer films[9] as well as minority carrier lifetime in silicon.[10] Contact SPM methods such as photoconductive-AFM have also been recently developed to characterize organic photovoltaic cells.,[1112] But none of the above methods would be able to map the carrier lifetime with the required high spatial resolution.

In this Letter, we present a novel measurement method that combines a time-resolved spectroscopy method, respective photoinduced transient spectroscopy (PITS), with scanning probe microscopy, which we call scanning probe photoinduced transient spectroscopy (PITS-SPM). Photoconductance decay and photoinduced transient spectroscopy are methods developed at the eve of the semiconductor physics and technology to characterize the electronic properties of semiconductors, especially lifetime and trap states in the band gap.[13,14] PITS uses light pulses to excite ehp and to study the decay of photoelectric currents after the cessation of the optical excitation. It gives information on the recombination lifetime

Received: October 21, 2011
Revised: March 29, 2012
Published: April 2, 2012

and a temperature-dependent study allows to determine trapping levels in the band gap even with a certain spatial resolution limited by the excitation beam.[15−17]

We show here that it is possible using PITS-SPM to experimentally determine the generation and recombination lifetime and map both lifetimes with nanoscale resolution which is limited only by the AFM tip−sample contact diameter. We also show here that in the case of $BiFeO_3$ the recombination processes within the ferroelectric domains are not significantly different from those in the proximity of the domain walls, invalidating in this way the initial PV model in $BiFeO_3$.

We have taken the advantage of a significant tip-enhancement of the photovoltaic currents in the photoelectric atomic force microscope[18] and introduced time-resolved photovoltaic measurements, by slightly modifying the experimental setup (see Figure S1 of Supporting Information). The illumination of the sample, here a (100)-oriented BFO single crystal, is now performed with laser pulses (405 nm wavelength) having defined amplitude, width, and repetition rate. The AFM tip is used to collect the local photovoltaic current, which is then amplified with a wide band (400 kHz) current amplifier.

Figure 1 shows the waveforms of the incident light and the photovoltaic current collected by the AFM tip. Few very

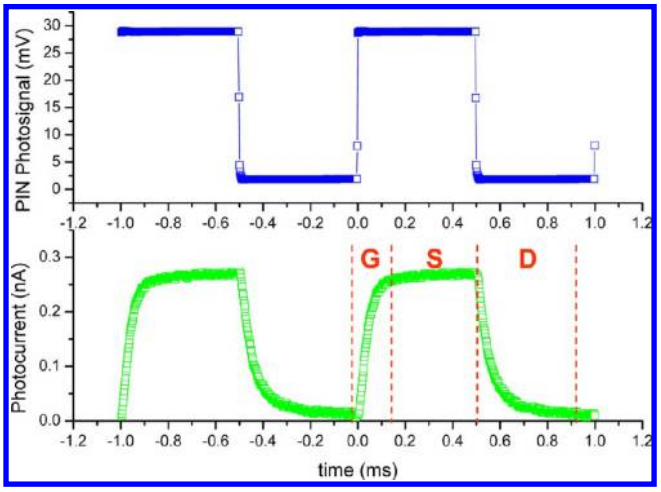

Figure 1. Local photovoltaic response of a (100)-oriented BFO single crystal to a rectangular type illumination with a laser of 405 nm wavelength. (a) Light excitation waveform as detected by a high speed PIN photodiode and (b) photovoltaic current collected through an AFM tip from a (100)-oriented BFO single crystal. The generation *G*, steady-state *S*, and the decay part *D* of the PV signal are also shown. The measured current should in principle be a superposition of photovoltaic current and pyroelectric current. In the present case the pyroelectric contribution should be about 6 orders of magnitude lower than the photovoltaic current (see SOM).

important observations can be already drawn from the time dependence of the PV current. While the on and off switching speed of the exciting light is high (the rise and decay times of the laser are shorter than few microseconds), the short circuit photovoltaic current follows the illumination with an obvious longer response time. This suggests that the mechanism of the PV current is not a simple band−band excitation mechanism but it should involve (shallow) trap levels that capture and re-emit charges according to their time constant, respectively cross-section. Shallow traps are known to cause longer rise time according to the ratio between free and trapped carriers.[19] The same applies for the decay part of the signal when not only the free carriers but also the trapped carriers have to recombine.

The photovoltaic response can be analyzed assuming the case of an ideal insulator in which the density of thermally generated carriers is much lower than the density of the photoinduced carriers. In this case, the simplest rate equation can be considered[20]

$$\frac{\partial n(t)}{\partial t} = G - R = G - \frac{n(t)}{\tau_{\text{eff}}} \tag{1}$$

where $n(t)$ is the carrier density at the time t, G and R are the generation and recombination rates, respectively, and τ_{eff} is the effective time constant. The photocurrent is proportional to the density of photoexcited carriers $n(t)$.

Three main time domains can be separated from this general time behavior of the PV signal. The rise part immediately after the light is switched on (region G in Figure 1), where the current increases rapidly from zero to the maximum value, is associated with carrier generation. Here the generation rate is much higher than the recombination rate thus the carrier density rate should be positive. The solution of (1) describing an exponential rise of the current is of the following form

$$n(t) = G\tau_{\text{g}}\left[1 - \exp\left(\frac{t}{\tau_{\text{g}}}\right)\right] \tag{2}$$

The characteristic response time is here the generation time constant or the generation lifetime τ_{g}. Region *S* is the steady-state region in which the carrier density is constant in time. The generation and recombination rates are equal. The carrier density follows a simple form

$$n(t) = G\tau \tag{3}$$

After the light excitation ceases, the generation rate G becomes zero and only recombination processes are taking place. The carrier density is described by the following equation

$$n(t) = G\tau_{\text{r}} \exp\left(-\frac{t}{\tau_{\text{r}}}\right) \tag{4}$$

where now τ_{r} is the effective recombination lifetime. In the case of an ideal semiconductor, the generation and recombination lifetimes should be identical. In a more general case, when the generation and recombination mechanisms involve one or more energy levels in the band gap, the recombination lifetime can be different from the generation lifetime.[21]

The effective generation and recombination lifetime can be determined by fitting the experimental data with the rate equation. As Figure 2 shows, the fit of the rise part of the PV signal with (2) is very good, giving an effective generation lifetime of 35 μs. The decay part of the signal can be analyzed by using (4). A main recombination lifetime of about 75 μs governs the signal in the decay part just after the cessation of the excitation. The signal tail obeys the same exponential decay with a much longer lifetime of about 1.5 ms. An important conclusion can be drawn from the above analysis: generation-recombination processes in this case are not simple band−band processes. Usually the band−band excitation is very fast and a longer generation lifetime is mostly due to a more complex process that involves trapping and thermal activation processes to and from shallow energy levels in the band gap. The same applies to the recombination processes that in addition show two exponential decays times. The two distinct recombination

dx.doi.org/10.1021/nl300618e | *Nano Lett.* 2012, 12, 2193−2198

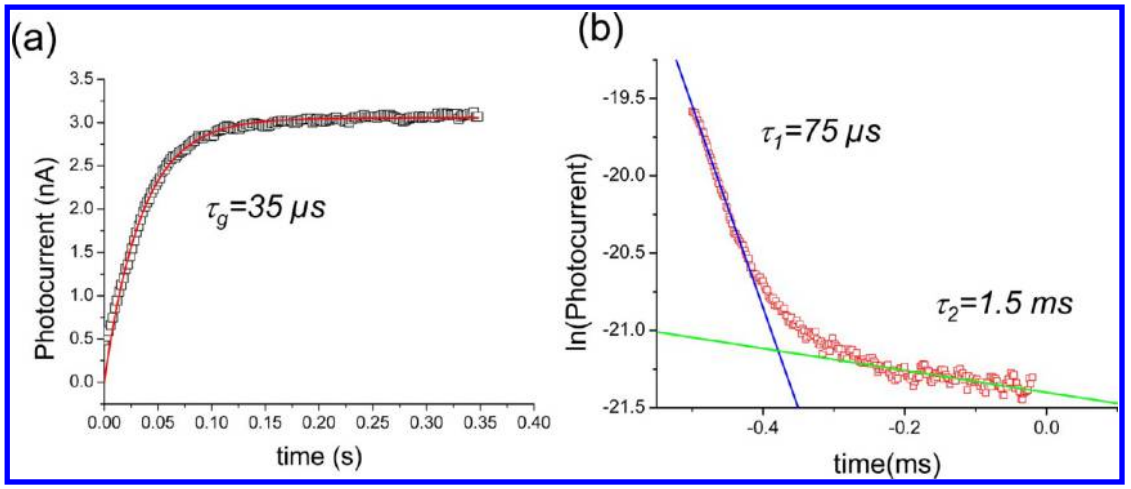

Figure 2. Photovoltaic current in the (a) generation *G* and (b) decay *D* part of the signals. The solid lines are fits with eqs 2 and 4 in (a) and (b), respectively. The effective generation and recombination times are marked.

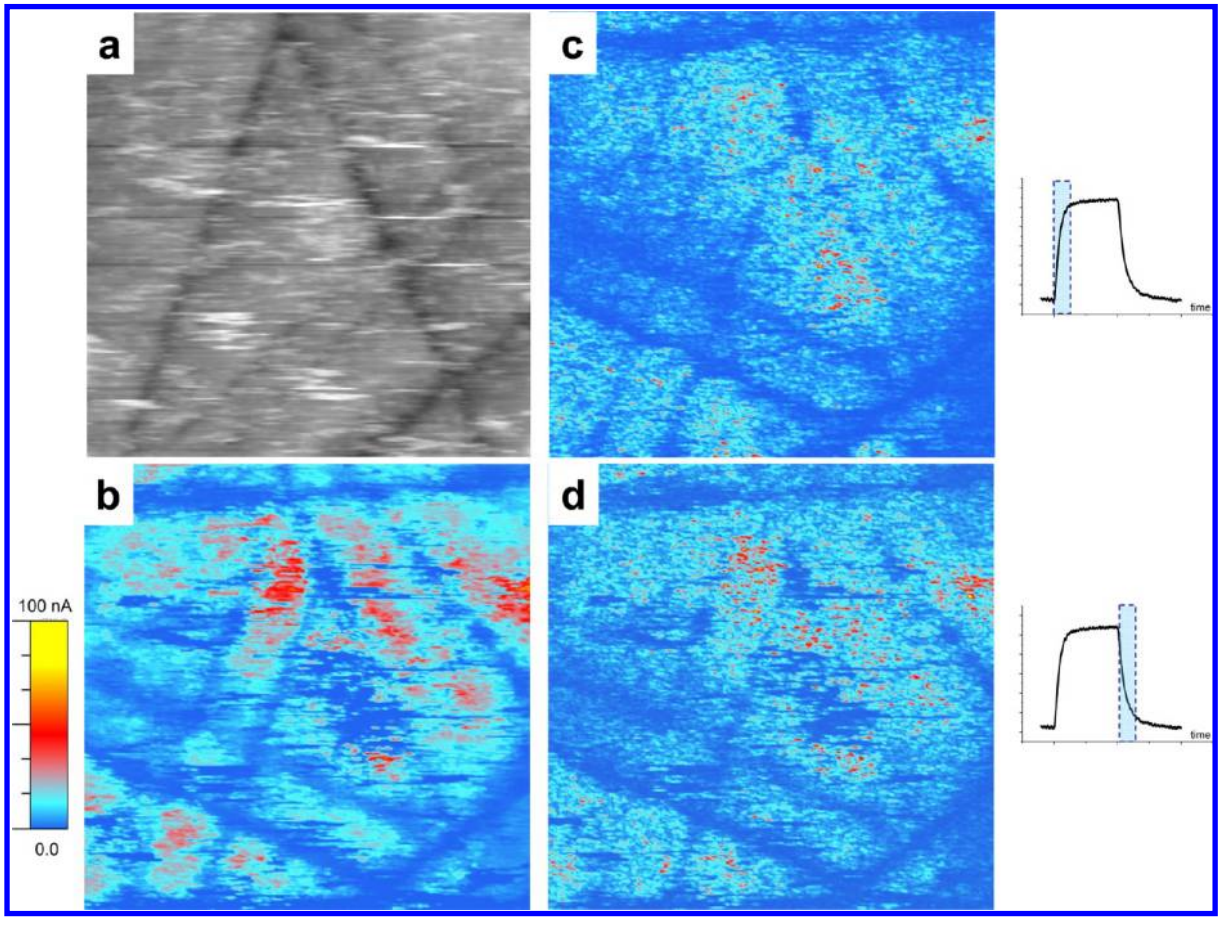

Figure 3. Local mapping of photoconductive and PITS signals of a (100)-oriented CdS single crystal. (a) Topography, (b) dc photoconductive signal, (c) PITS signal at the rise edge, and (d) PITS signal at the decay edge. The position of the acquisition window of the PITS signals is schematically shown in insets of (c) and (d). The photoconductive and PITS signals have been acquired under 4 V external applied voltage on the AFM tip. The scan area is 5 × 5 μm^2.

lifetimes can be due to a more complicated recombination process with two independent Shockley–Read–Hall (SRH) centers with different recombination rates.[22] Alternatively the recombination processes for electrons and holes can lead to a different effective lifetime for each carrier type, which is the usual case of insulators.[19] The different generation and recombination lifetimes suggest a more complex mechanism involving at least two shallow trapping levels with distinct trapping and re-emission rates. This is also suggested by the dependence of the lifetime on the incident light intensity, which decreases by increasing the light intensity, as in the case of CdS.[23]

It should be recalled that the photocurrent analyzed above is not only detected without any applied external voltage but also

dx.doi.org/10.1021/nl300618e | *Nano Lett.* 2012, 12, 2193–2198

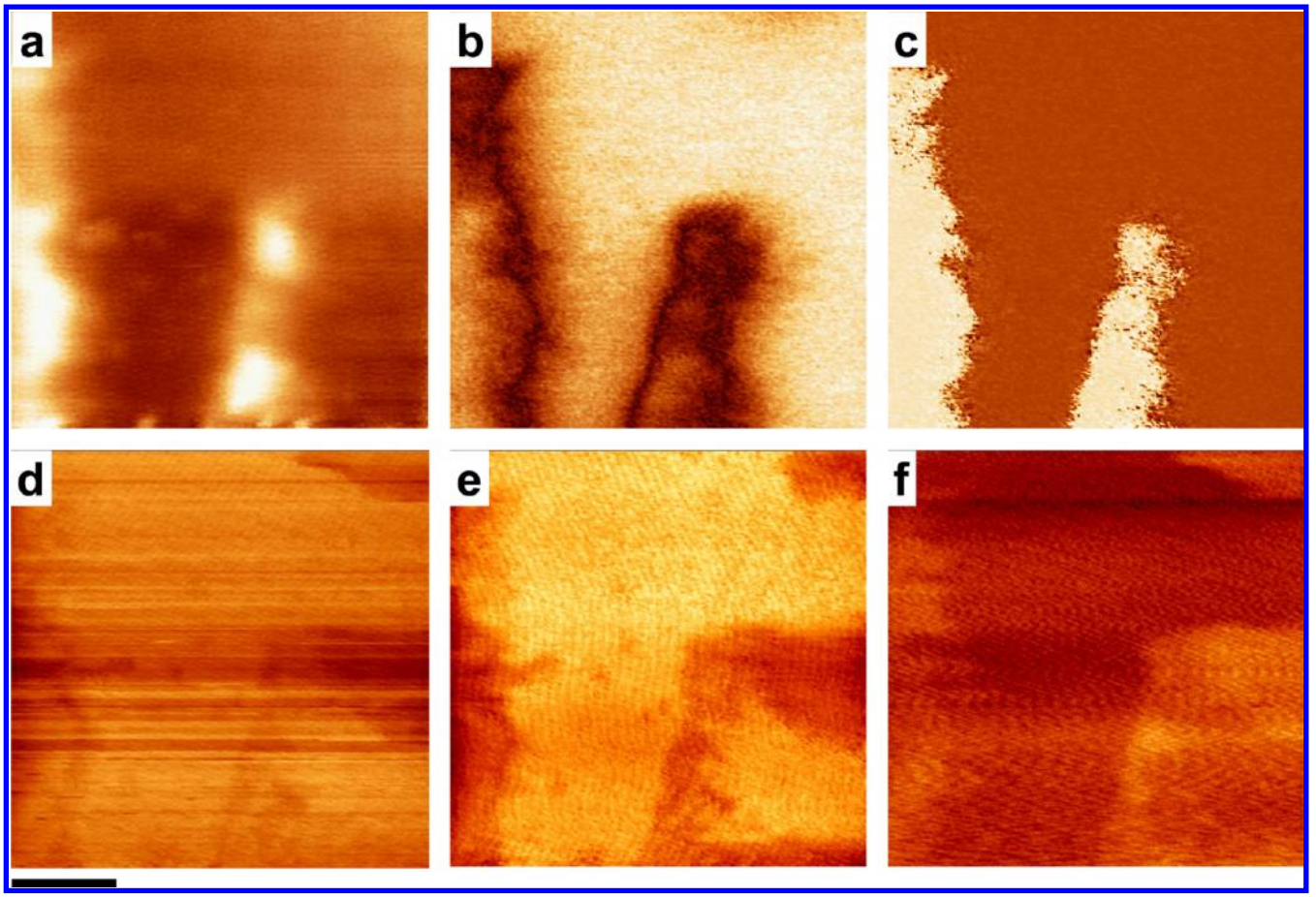

Figure 4. Ferroelectric domains, photovoltaic, and lifetime maps of a BFO single crystal. A 1 × 1 μm^2 scan showing (a) topography, (b) out-of-plane PFM amplitude, (c) out-of-plane PFM phase signal, (d) dc photovoltaic signal, (e) rise-PITS (generation) signal, and (f) decay-PITS (recombination) signal maps. The domain walls are easily seen as the dark contrast lines in (b). All signals are in arbitrary units. The lower left scale is 250 nm.

through an AFM conductive tip. Thus, it should in principle be possible to perform the above analysis while scanning the tip over the sample surface and correlate the above generation and recombination lifetimes with the tip position on the surface. It can thus in principle be possible to correlate the generation-recombination properties with other relevant properties such as surface defects or ferroelectric polarization orientation and/or domain pattern in the case of ferroelectrics. A real-time detailed analysis as above while scanning the tip over the surface will be rather impossible. Therefore, we have developed a special analogue electronic circuit which gives information on the lifetime as an output voltage signal. This circuit allows selection of any part *G*, *S*, or *D* of the photovoltaic signal. As shown schematically in Supporting Information Figure S2, a triggered switch opens for a determined time t_{window}. A delay circuit synchronized with the laser pulse allows selecting the desired part of the PV signal by adjusting the delay time t_{delay}. This so-called PITS signal is then fed into a lock-in amplifier which by integration of many excitation cycles will deliver a voltage signal that can be interpreted in terms of lifetime. The effective frequency at which the system can work is determined chiefly by the speed at which the sample responds to the light excitation. For fast generation-recombination processes, the frequency is as high as 10 kHz, allowing an integration time constant of the order of 1 ms, similar to other AFM-based ac measurements such as piezoresponse force microscopy (PFM). For the particular signals shown in Figure 1, where the excitation frequency is about 2 kHz, a lock-in integration time constant of about 3 ms and scanning rate of 0.5 s were found to be appropriate parameters to achieve a real time mapping of the PITS signals. It is thus possible to have a real time mapping of the PITS signals proportional to the signals in either the generation or recombination part, imaging thus generation and recombination lifetimes. As we mentioned, this gives the possibility to correlate carrier lifetime to surface defects revealed by topography images or with polarization orientation and/or domain walls in ferroelectrics determined by PFM in a successive measurement.

Before measuring the ferroelectric BFO system, we have verified the above concept and measurement setup using a CdS single crystal. CdS is one of the most known photoconductive materials and has a band gap of 2.4 eV, close to the BFO band gap. Figure 3 shows the dc photoconductive (PC) and PITS signals acquired from a randomly oriented CdS single crystal. The PITS signals and images should be interpreted as follows (see also Supporting Information Figure S3): at the decay part of the signal (d-PITS) a high recombination rate (short effective lifetime) will generate a very abrupt decay signal. The signal delivered by the lock-in amplifier, that is, the PITS signal that is mapped would be thus smaller for a high recombination rate. The opposite applies for the rise part of the signal (r-PITS). A high PITS signal should be interpreted either as a

dx.doi.org/10.1021/nl300618e | *Nano Lett.* 2012, 12, 2193−2198

large generation rate or a shorter effective generation lifetime. The generation rate and/or lifetime can vary from point to point and this might induce a false interpretation of the spatial distribution of the recombination lifetime. A low generation rate will give both low generation and recombination PITS signals, whereas an obvious recombination center would be a region with a normal generation rate, but low PITS decay signal. Thus, a proper interpretation of the decay d-PITS images should always be related to the image of the rise r-PITS signal or the dc photocurrent image, as in the case of dynamic carrier lifetime imaging in silicon.[24] Actually, the PITS signals should always be evaluated considering both rise and decay parts, as suggested in early work.[25] It is even possible to subtract or normalize the recombination signals to the generation signals to enhance the contrast, as shown in Supporting Information Figure S4, for the CdS case.

The PC and PITS images in Figure 3 show essentially that some visible surface defects degrade significantly the effective generation rate and thus the dc photoconductive signal. There are also some regions with low generation rate that are not connected to any visible surface defect, as well as regions in which the photoconductive signal is very low just due to strong recombination, as can be easily seen in the middle of the scan area. These latter can be considered as recombination centers.

The above CdS example shows that it is possible to detect recombination centers with a very high lateral resolution limited only by the tip−surface contact diameter, like in many other scanning probe measurements.

Applying the above technique to BFO single crystals will give the possibility to detect and map the recombination centers and thus gain an insight into the microscopic mechanism of the abnormal photovoltaic effect shown by this material. Figure 4 shows the dc photovoltaic, PITS, and PFM signals mapped on an area with a typical domain structure showing a micrometer-large area in which ferroelastic domains are running across. Similar as in our previous work (ref 18) the domains are 109° ferroelastic domains revealed by contrast in both out-of-plane and in-plane (not shown) PFM images. The dc photovoltaic and PITS signals are rather uniform and the contrast in respective images represents maximum 30% of the average signals. The dc PV signal (Figure 4d) shows a slightly lower PV current within the domains with polarization pointing upward. A similar contrast is present in the generation rate given by the map of the r-PITS signal (Figure 4e). This image shows a good correlation between the domains and regions having low generation rate and lifetime. The image of the decay PITS signals (Figure 4f), which should be associated with the recombination lifetime, shows that areas with low PV signals are associated with high r-PITS signals, that is, with a long decay time. This is somehow different than in the case of common semiconductors where a long lifetime is normally associated with larger photoelectric signals. The long decay time should here be interpreted together with the long generation time. As mentioned, a longer generation lifetime is mostly due to a more complex electronic mechanism involving shallow levels in the band gap. In such a way, the Figure 4f maps actually the distribution of the trapping levels rather than the true recombination lifetime. It reveals that the regions with high contrast, representing a longer effective lifetime, are associated with the domains with polarization pointing upward. These areas are connected but not restricted to the ferroelectric domains or domain walls, as it can be readily seen also in Supporting Information Figure S5, where there is contrast unrelated to any ferroelectric domain. Such an influence of the polarization on the trapping effects in BFO has recently been reported by Lee et al.,[26] who assumed oxygen vacancies to be at the origin of this effect. However, because the PITS signals are rather uniform we can draw the conclusion that the effective recombination lifetime is not markedly smaller in the bulk of the domains compared to the regions near to the domain walls. Likewise, the generation lifetime of 35 μs is rather constant and very long compared to the previously assumed values of a few picoseconds.[7]

In conclusion, we have developed a novel scanning probe microscopy method employing photoinduced transient spectroscopy (PITS-SPM) that is able to map the generation and recombination lifetime with high lateral resolution. This is a generic method that can be used to map and detect recombination centers on any photoelectric material and it is relatively easy to implement to any atomic force microscope. Here it has been successfully applied on a typical photoconductor material (CdS) as well as to $BiFeO_3$ single crystals. The combined investigations of PV effects and PITS-SPM on BFO single crystals strongly suggest that the role of the domain walls in the mechanism of the photovoltaic signal in BFO is different than initially proposed. The generation and recombination lifetime are very large and are not very different within the domain compared to domain walls. It has been found that the generation rate is slightly lower at the domain walls than in the bulk. This might be related to a higher dark conductivity of the domain walls,[2728] which would actually act as shunts lowering the photovoltaic signal.

■ ASSOCIATED CONTENT

Ⓢ Supporting Information

Supporting figures. This material is available free of charge via the Internet at http://pubs.acs.org.

■ AUTHOR INFORMATION

Corresponding Author

*E-mail: malexe@mpi-halle.de.

Notes

The authors declare no competing financial interest.

■ ACKNOWLEDGMENTS

The present work was partly supported by the German science foundation (DFG) through SFB762. The author thanks Dietrich Hesse and Otwin Breitenstein for critical reading and Detlef Proske for technical help.

■ REFERENCES

(1) Catalan, G.; Scott, J. F. *Adv. Mater.* **2009**, *21* (24), 2463−2485.
(2) Kundys, B.; Viret, M.; Colson, D.; Kundys, D. O. *Nat. Mater.* **2010**, *9*, 803−805.
(3) Choi, T.; Lee, S.; Choi, Y. J.; Kiryukhin, V.; Cheong, S. W. *Science* **2009**, *324* (5923), 63−66.
(4) Yi, H. T.; Choi, T.; Choi, S. G.; Oh, Y. S.; Cheong, S. W. *Adv. Mater.* **2011**, *23* (30), 3403−3407.
(5) Yang, S. Y.; Seidel, J.; Byrnes, S. J.; Shafer, P.; Yang, C. H.; Rossell, M. D.; Yu, P.; Chu, Y. H.; Scott, J. F.; Ager, J. W.; Martin, L. W.; Ramesh, R. *Nat. Nanotechnol.* **2010**, *5* (2), 143−147.
(6) Yang, S. Y.; Martin, L. W.; Byrnes, S. J.; Conry, T. E.; Basu, S. R.; Paran, D.; Reichertz, L.; Ihlefeld, J.; Adamo, C.; Melville, A.; Chu, Y. H.; Yang, C. H.; Musfeldt, J. L.; Schlom, D. G.; Ager, J. W.; Ramesh, R. *Appl. Phys. Lett.* **2009**, *95*, 062909.
(7) Seidel, J.; Fu, D. Y.; Yang, S. Y.; Alarcon-Llado, E.; Wu, J. Q.; Ramesh, R.; Ager, J. W. *Phys. Rev. Lett.* **2011**, *107*, 126805.

(8) Sturman, B. I.; Fridkin, V. M. *The Photovoltaic and Photorefractive Effects in Noncentrosymmetric Materials*; Gordon and Breach: Philadelphia, 1992.
(9) Coffey, D. C.; Ginger, D. S. *Nat. Mater.* **2006**, *5* (9), 735−740.
(10) Takihara, M.; Takahashi, T.; Ujihara, T. *Appl. Phys. Lett.* **2008**, *93*, 021902.
(11) Dante, M.; Peet, J.; Nguyen, T. Q. *J. Phys. Chem. C* **2008**, *112* (18), 7241−7249.
(12) Pingree, L. S. C.; Reid, O. G.; Ginger, D. S. *Nano Lett.* **2009**, *9* (8), 2946−2952.
(13) Stevenson, D. T.; Keyes, R. J. J. *Appl. Phys.* **1955**, *26*, 190−195.
(14) Hurtes, Ch.; Boulou, M.; Mitonneau, A.; Bois, D. *Appl. Phys. Lett.* **1978**, *32*, 821−823.
(15) Yoshie, O.; Kamihara, M. *Jpn. J. Appl. Phys.* **1983**, *22*, 621−628.
(16) Yoshie, O.; Kamihara, M. *Jpn. J. Appl. Phys.* **1985**, *24*, 431−440.
(17) Breitenstein, O.; Giling, L. J. *Phys. Status Solidi A* **1987**, *99*, 215−219.
(18) Alexe, M.; Hesse, D. *Nat. Commun.* **2011**, DOI: DOI: 10.1038/ncomms261.
(19) Rose, A. *Phys. Rev.* **1955**, *97*, 322−333.
(20) Bube, R. H. *Photoelectronic properties of semiconductors*; Cambridge University Press: Cambridge, U.K., 1992; Chapter 2.
(21) Schroder, D. K. *IEEE Trans. Electron Devices* **1982**, *29*, 1136−1139.
(22) Bube, R. H. *Photoelectronic properties of semiconductors*; Cambridge University Press: Cambridge, U.K., 1992; Chapter 4.
(23) Bube, R. H. *Solid-State Electron.* **1984**, *27*, 467−73.
(24) Ramspeck, K.; Reissenweber, S.; Schmidt, J.; Bothe, K.; Brendel, R. *Appl. Phys. Lett.* **2008**, *93*, 102104.
(25) Fairman, R. D.; Morin, F. J.; Olivier, J. R. *Inst. Phys. Conf. Ser.* **1979**, *45*, 134−143.
(26) Lee, W.-M.; Sung, J. H.; Chu, K.; Moya, X.; Cho, Y.-J.; Kim, C.-J.; Mathur, N.D.; Cheong, S.-W.; Yang, C.-H.; Jo, M.-H. *Adv. Mater.* **2012**, DOI: DOI: 10.1002/adma.201102816.
(27) Seidel, J.; Martin, L. W.; He, Q.; Zhan, Q.; Chu, Y. H.; Rother, A.; Hawkridge, M. E.; Maksymovych, P.; Yu, P.; Gajek, M.; Balke, N.; Kalinin, S. V.; Gemming, S.; Wang, F.; Catalan, G.; Scott, J. F.; Spaldin, N. A.; Orenstein, J.; Ramesh, R. *Nat. Mater.* **2009**, *8* (3), 229−234.
(28) Guyonnet, J.; Gaponenko, I.; Gariglio, S.; Paruch, P. *Adv. Mater.* **2011**, DOI: 10.1002/adma.201102254.